AD-A113 753 UNITED TECHNOLOGIES RESEARCH CENTER EAST HARTFORD CT F/G 20/7
INVESTIGATION OF ELECTRON COLLISION PROCESSES IN HGBR2.(U)
APR 82 W L NIGHAN, J J HINCHEN, W J WIEGAND N00014-81-C-0253
UNCLASSIFIED R82-525545-1 NL

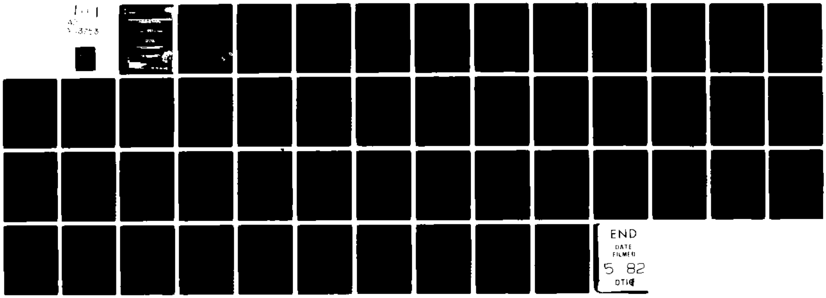

END
DATE
FILMED
5 82
DTIC

R82-925545-1

Investigation of Electron Collision Processes in $HgBr_2$

Final Report
April 14, 1982

Prepared by

William L. Nighan
John J. Hinchen
Walter J. Wiegand

Sponsored by the Naval Ocean Systems Center
Under Contract N00014-81-C-0253

United Technologies Research Center
East Hartford, Connecticut 06108

Unclassified

SECURITY CLASSIFICATION OF THIS PAGE (When Data Entered)

REPORT DOCUMENTATION PAGE

READ INSTRUCTIONS BEFORE COMPLETING FORM

1. REPORT NUMBER R82-525545-1	2. GOVT ACCESSION NO. AD-A113 753	3. RECIPIENT'S CATALOG NUMBER
4. TITLE (and Subtitle) Investigation of Electron Collision Processes in $HgBr_2$		5. TYPE OF REPORT & PERIOD COVERED Final Report Feb. 15, '81-April 14, '82
		6. PERFORMING ORG. REPORT NUMBER R82-525545-1
7. AUTHOR(s) William L. Nighan, John J. Hinchen and Walter J. Wiegand		8. CONTRACT OR GRANT NUMBER(s) N00014-81-C-0253
9. PERFORMING ORGANIZATION NAME AND ADDRESS United Technologies Research Center Silver Lane East Hartford, CT 06108		10. PROGRAM ELEMENT, PROJECT, TASK AREA & WORK UNIT NUMBERS
11. CONTROLLING OFFICE NAME AND ADDRESS Office of Naval Research Physics Program Office 800 No. Quincy St., Arlington, VA 22217		12. REPORT DATE April 14, 1982
		13. NUMBER OF PAGES 47
14. MONITORING AGENCY NAME & ADDRESS(if different from Controlling Office)		15. SECURITY CLASS. (of this report) Unclassified
		15a. DECLASSIFICATION/DOWNGRADING SCHEDULE

16. DISTRIBUTION STATEMENT (of this Report)

Approved for public release; distribution unlimited.
Reproduction in whole or in part is permitted for any purpose of the United States Government.

17. DISTRIBUTION STATEMENT (of the abstract entered in Block 20, if different from Report)

18. SUPPLEMENTARY NOTES

This final report is based on a manuscript which has been submitted for publication in the Journal of Chemical Physics.

19. KEY WORDS (Continue on reverse side if necessary and identify by block number)

$HgBr_2$ Ionization, $HgBr_2$ Dissociative Attachment, $HgBr_2$ Vibrational Excitation, Electron-$HgBr_2$ Cross Sections, Electron Drift Velocity in $HgBr_2$, HgBr Lasers, $HgBr_2$ Dissociation Laser

20. ABSTRACT (Continue on reverse side if necessary and identify by block number)

Cross sections for mercuric bromide ($HgBr_2$) dissociative attachment and ionization have been measured using an electron beam experiment. The dominant products of these reactions, as identified by mass analysis, are $Br^{(-)}$ and $HgBr_2^{+}$. A complementary electron swarm experiment was used to determine the ion production coefficients in a variety of gas mixtures containing $HgBr_2$. The measured ion production coefficients were found to be in excellent agreement with the attachment and ionization coefficients computed using the

DD FORM 1 JAN 73 1473 EDITION OF 1 NOV 65 IS OBSOLETE

S/N 0102-LF-014-6601

Unclassified

SECURITY CLASSIFICATION OF THIS PAGE (When Data Entered)

Hg Br2 (+3)

measured cross sections. Additionally, analysis of the variations in the measured $HgBr_2$ ion production coefficients along with measured electron drift velocity variations is found to be consistent with the interpretation that vibrational excitation of $HgBr_2$ is dominated by a resonance in the 3-5 eV electron energy range for which dissociative attachment is observed to occur.

Accession For	
NTIS GRA&I	☑
DTIC TAB	☐
Unannounced	☐
Justification	
By	
Distribution/	
Availability Codes	
Dist	Avail and/or Special
A	

PREFACE

Under the present contract United Technologies Research Center has carried out a basic experimental and analytical investigation of low energy electron collision phenomena in $HgBr_2$. Cross sections for mercuric bromide ($HgBr_2$) dissociative attachment and ionization have been measured using an electron beam experiment. The dominant products of these reactions as identified by mass analysis, are Br^- and $HgBr_2^+$. A complementary electron swarm experiment was used to determine the ion production coefficients in a variety of gas mixtures containing $HgBr_2$. The measured ion production coefficients were found to be in excellent agreement with the attachment and ionization coefficients computed using the measured cross sections. Additionally, analysis of the variations in the measured $HgBr_2$ ion production coefficients along with measured electron drift velocity variations is found to be consistent with the interpretation that vibrational excitation of $HgBr_2$ is dominated by a resonance in the 3-5 eV electron energy range for which dissociative attachment is observed to occur.

This investigation was closely coordinated with other complementary Corporate and Navy supported experimental and theoretical programs, particularly Contracts N00014-80-C-0247 and N00014-76-C-0847. The present final report is based on a manuscript which has been submitted for publication to the Journal of Chemical Physics.

R82-925545-1

Investigation of Electron Collision Processes in $HgBr_2$

TABLE OF CONTENTS

I. INTRODUCTION

The 502 nm HgBr(B→X) laser is a leading candidate for applications requiring an efficient (>1%) visible laser capable of generating relatively high average power (>100W)[1]. Mercuric bromide, $HgBr_2$, is the source of mercurous bromide in this electrically excited laser. Modeling of this laser requires knowledge of the low energy electron $HgBr_2$ cross sections for such processes as attachment, ionization, and vibrational and electronic excitation. In this paper we report the results of an experimental and analytical investigation directed toward determination of certain of these cross sections.

Two entirely independent, albeit complementary, experimental techniques were used in this investigation[2]: low energy electron-beam measurements and electron swarm measurements. Section II presents a description of electron beam measurements of the e-$HgBr_2$ cross sections for dissociative attachment and for ionization. The principal ion products of these reactions, as identified by mass analysis, were found to be Br^- and $HgBr_2^+$, respectively. A complementary electron swarm experiment used to determine the corresponding electron rate coefficients for attachment and ionization is described in Section III. The measured rate coefficients were found to be in excellent agreement with those computed using the e-beam measured cross sections. In addition, measurements of the electron drift velocity in rare gas - $HgBr_2$ mixtures were analyzed in order to obtain information concerning vibrational excitation of $HgBr_2$ by electrons. This analysis showed that the measured variations in the electron drift velocity and attachment coefficient are consistent with the interpretation that vibrational excitation of $HgBr_2$ is dominated by a resonant excitation process in the 3-5 eV electron energy range for which dissociative attachment is also observed to occur.

II. ELECTRON BEAM MEASUREMENTS

A. Technique

Refinements to the classic Tate-Smith[3] electron beam method by Rapp and co-workers[4-6] have provided an abundance of data concerning ionization and attachment of numerous atmospheric and rare gases, while additional works by Chantry[7] and by Kurepa, et al[8,9] report cross sections for several electronegative species.

The method consists of firing a magnetically collimated electron beam through a nearly electric field-free collision chamber containing the subject gas at a known concentration. Ions formed as a result of ionizing or attaching collisions are not greatly influenced by the applied magnetic field, and under the influence of a weak transverse electric field are collected on electrodes located at opposite sides of the collision chamber. Due to their small Larmor radii, scattered electrons cannot reach these collectors and are intercepted by the chamber end walls. The remaining beam electrons are collected on an electrode located beyond the chamber. The cross section, Q, for the process of interest is computed from the measured ion current, I_I, electron-beam current, I_e, gas concentration N, and beam path length, L, using the simple expression:

$$Q = I_I/(I_e NL) \quad . \tag{1}$$

Additional information regarding the ion formation processes is obtained by mass analysis of sampled product ions.

B. Apparatus

In the present investigation a beam experiment in the Tate-Smith configuration was used, with ion analysis provided by a quadrupole mass spectrometer. The collision chamber and mass spectrometer were housed in a stainless steel vacuum chamber whose 10^{-7} torr base pressure was maintained by a LN_2 trapped diffusion pump. The system including the collision chamber and spectrometer was superheated to 390°K to preclude the possibility of forming secondary $HgBr_2$ reservoirs. The mercuric bromide powder initially was vacuum distilled into the primary reservoir where a temperature stabilized warm water bath controlled the $HgBr_2$ vapor pressure[10] during subsequent data acquisition.

Collision Chamber Design

The collision chamber assembly replaced the commercial ionizer section on the quadrupole mass spectrometer. The principal features of the chamber design are illustrated in Fig. 1 which also shows a typical potential profile. The source consisted of a dc heated thoriated iridium filament, FILA, an electron extracting electrode, EXTR, and a retarding potential difference plate, RPD. The EXTR and RPD potentials were referenced with respect to the center potential of the filament, which was swept negatively relative to the collision chamber, CHAMB, to provide a beam of increasingly energetic electrons. Depending on the potential of the RPD plate relative to the filament voltage, the beam source could be operated as a conventional electron source or, for high resolution measurements, in the RPD mode[11,12] where the voltage increment was provided on alternate electron energy sweeps.

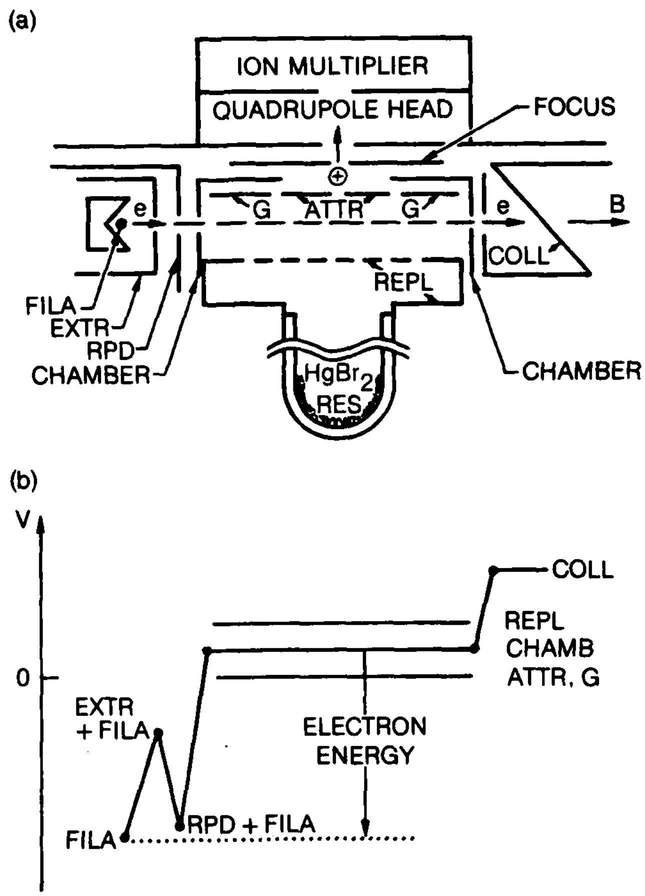

Fig. 1. Schematic illustration of the collision chamber (a), and a typical voltage profile along the electron beam path (b). The voltage profile (b) is representative of a positive ion tune. For negative ion observation the polarities of REPL and CHAMB are reversed. Beam energy, sweep, and RPD programming were keyboard controlled from a DEC PDP 11 computer which, in conjunction with a Tracor Northern multichannel analyzer, served to process the acquired data. An MKS Baratron capacitive pressure transducer measured the pressure at a location intermediate between the reservoir and the collision chamber.

82-3-139-1

The electron beam was constrained to a nearly linear path in the collision chamber by a field of up to 600 Gauss provided by external electromagnets. The collision chamber proper comprised four electrically isolated elements: the chamber piece, CHAMB, that contained the beam entrance and exit apertures at a separation of 3.34 cm; the repeller, REPL, that consisted of a perforated sidewall backed by a small plenum coupled to the reservoir tube; the attractor, ATTR, with its ion sampling aperture; and the split guard electrode, G, that minimized leakage currents and defined the 1.10 cm ion collection length of the attractor. The chamber elements were precision formed from 0.25 mm stainless steel stock, insulated from each other by shielded alumina spacers and, when assembled into the collision chamber, constituted an enclosure from which the loss of vapor occurred principally through the beam apertures. Finally, the collector electrode, COLL, was configured such as to minimize the possibility of reflected or secondary electrons returning to the collision chamber.

Collision chamber electrode voltages were tuned to sustain the potential on the electron beam path within the chamber at a level equal to the potential applied to the chamber end faces, while a sufficient transverse field was maintained between the repeller and attractor/guard electrodes to saturate ion current collection. To permit observation of the ions by the quadrupole spectrometer whose entrance aperture was grounded, the chamber voltage was biased typically several volts positive or negative depending on the polarity of ions under study. The attractor and collector currents were measured with Keithley electrometers in series with a bias battery. Selectively, the output signals from either of the electrometers could be sent to a multichannel analyzer/DEC PDP 11 controller system for subsequent evaluation of the cross sections.

Products of the electron-$HgBr_2$ collisions were identified by extracting a portion of the attractor-directed ion current through an aperture in that electrode. The Electronic Associates Quad 200 Residual Gas Analyzer utilized for mass analysis was equipped with a Channeltron 4039 (Ruggedized) ion multiplier that was used in the pulse counting mode. Since multiplier gain deteriorated during measurements of $HgBr_2$ fragment ions, observation at the lowest feasible chamber pressure and sampling current level was required.

C. System Calibration

Absolute energy scales and magnitudes for the cross sections were established by system calibrations employing krypton and xenon, whose ionization cross sections are well known[4]. At the submillitorr pressures of these studies, free molecular flow considerations indicate that while the loss rate of gas from the chamber is mass dependent, the ratio of the pressure as measured at the Baratron gauge to that existing in the collision chamber remains species independent[4]. To determine this ratio, Xe and Kr were separately leaked through the reservoir into the chamber to various gauge pressures in the 10^{-4}-10^{-2} torr range. The energy dependence of the measured attractor-to-beam current ratio ($I_I/I_e \propto Q_i$) was found to duplicate that measured by Rapp and Englander-Golden[4]. Using the reported magnitudes of Q_i at 70 eV, the gas density, N, in the collision chamber was computed using Eq. 1. Comparison of this value with that determined from ($I_I/I_e \propto Q_i$) manometer readings established the apparatus calibration factor of 0.33 $\pm$ 0.03. Using this factor, $HgBr_2$ concentrations in the collision chamber were determined from the capacitance manometer readings during the mercuric bromide measurements.

The linear voltage sweep of the electron beam was calibrated to an absolute energy scale using current cut-off at zero energy and the well established[13] ionization thresholds of Xe and Kr.

D. $HgBr_2$ Ionization Cross Sections

The total electron impact cross section for ionization of mercuric bromide from threshold to 70 eV was determined from measurements using Eq. 1. Electron beam currents in the 10^{-8} A to low 10^{-7} A range were selected to eliminate space charge effects of the source. Attractor ion currents were limited to several percent of this beam current by setting reservoir temperatures to provide chamber densities between 10^{12} and 10^{13} cm^{-3}. Over these ranges of parameters, for all magnetic fields above 200 Gauss, and for reasonable variations in the chamber tune, the same $HgBr_2$ ionization cross section was extracted.

The measured total cross section for ionization of $HgBr_2$ is shown in Fig. 2 with tabulated values presented in Table I. As is typical of many gases, the ionization cross section is a generally featureless function of electron energy,

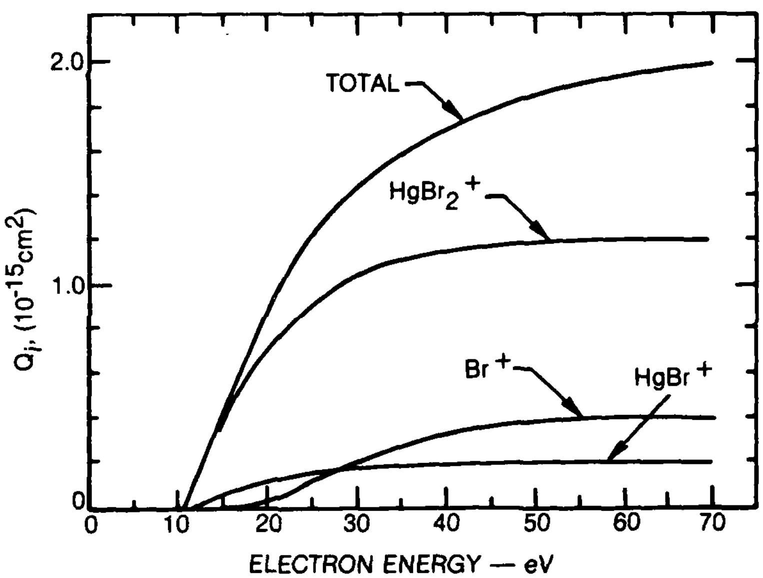

Fig. 2. Measured total and partial cross sections for electron impact ionization of $HgBr_2$.

82-3-139-2

rising nearly linearly from threshold (10.6 eV for $HgBr_2$) toward a maximum value at an energy above 70 eV. The measured ionization cross section is found to be very large, reaching a peak of about 2×10^{-15} cm^2 at 70 eV, a value estimated to have an accuracy of $\pm$ 25%. There are several correlations between the ionization cross section and the electron polarizability of molecules[14,15]. Consideration of the large value of $HgBr_2$ polarizability[16] (11.5Å^3), in light of these correlations, suggests a peak $HgBr_2$ ionization cross section in the range of 1 to 2×10^{-15} cm^2, a value in satisfactory agreement with the present measurement.

Partial Ionization Cross Sections

The simple appearance of the total ionization cross section belies the fact that it is a charge-weighted summation of a half-dozen partial cross sections, each having its own threshold and energy dependence. From mass spectrometer measurements information regarding these partial cross sections was determined. Ionization processes leading to the production of the singly charged ions $HgBr_2^+$, $HgBr^+$, Br^+, and Hg^+ contribute to the total ionization level at low electron energies, whereas $HgBr_2^{++}$, $HgBr^{++}$ and Br^{++} formation contribute to the net electron yield at high energies. Placing the partial cross sections on a true relative scale was not possible using the present beam experiment due to the unknown transmission efficiency of the ion extraction optics and the quadrupole mass spectrometer over such a broad ion mass range. Fortunately, relative abundances of $HgBr_2^+$, $HgBr^+$, Br^+ and Hg^+

produced from mercuric bromide have been measured[17] at 70 eV in a time-of-flight instrument wherein the response is relatively independent of ion mass. Using these published results to normalize the measured partial cross sections[17], the relative cross sections for the production of the several ions were estimated and are also shown in Fig. 2.

E. $HgBr_2$ Dissociative Attachment

Operation of the beam experiment with key potentials reversed permits determination of the cross sections for negative ion production. The total electron attachment cross section Q_a, in $HgBr_2$ was found to be resonant in character, consisting of a single peak located between 3.1 eV and 4.5 eV and centered at about 3.7 eV. Mass spectrometer analysis revealed that the process being observed was dissociative attachment leading to Br^- formation. The measured electron energy dependence of the attachment cross section is presented in Fig. 3 and Table I. The peak value of 1×10^{-17} cm^2 at 3.7 eV was determined in alternate calibrations of the peak attachment cross section and the total ionization cross section at 70 eV. These dual calibrations were obtained at common $HgBr_2$ reservoir temperatures over a range of $HgBr_2$ densities varying by a factor of ten and centered at a vapor concentration of 3×10^{12} cm^{-3}. Owing to uncertainties in the mercuric bromide chamber density, N, and the less than 10^{-11}A I_I current levels of these attachment measurements, the uncertainty of the peak attachment cross section is estimated to be approximately $\pm$ 30 percent.

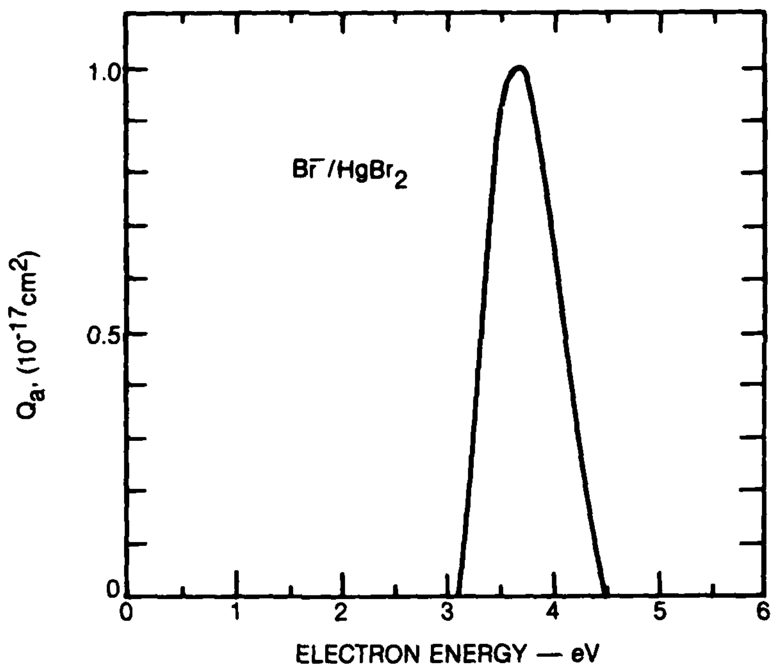

Fig. 3. Dissociative attachment cross section for electrons in $HgBr_2$; the negative ion product of this reaction is Br^-.

82-3-139-3

TABLE I. $HgBr_2$ CROSS SECTIONS FOR IONIZATION AND ATTACHMENT

Energy, eV	Q_i, 10^{-15} cm^2	Energy, eV	Q_a, 10^{-17} cm^2
10.62	0	3.1	0
12.5	0.18	3.2	0.18
15	0.41	3.3	0.4
17.5	0.64	3.4	0.7
20	0.88	3.5	0.9
22.5	1.09	3.6	0.98
25	1.23	3.7	1.0
30	1.44	3.8	0.96
35	1.58	3.9	0.85
40	1.7	4.0	0.67
45	1.79	4.1	0.5
50	1.85	4.2	0.35
55	1.91	4.3	0.22
60	1.95	4.4	0.1
70	2.0	4.5	0

III. ELECTRON SWARM EXPERIMENTS

A. Technique

An electron swarm experiment was used to provide a direct measure of the rate coefficients, k, for production or loss of electrons due to ionization or attachment reactions in $HgBr_2$. This independent technique is complementary to the electron-beam measurements described in the preceding section, and is especially useful when the cross section for a particular process has a narrow energy width, and/or has a measurable value only near zero energy as is frequently the case for attachment. In these circumstances the measurement of the electron energy-weighted cross section (i.e. the rate coefficient) can often provide a more accurate measure of the effective cross section magnitude than can beam measurements which may suffer from resolution problems.

The pulsed swarm technique used in the present studies is based on the integral method pioneered by Grünberg[18]. In this approach a burst of electrons is introduced into a constant electric field region between two parallel electrodes by photoemission from one electrode using a suitable light source. When a proper mixture of the attaching gas and a buffer is present in the interelectrode gap, attachment and/or ionization reactions convert a portion of the rapidly drifting electron group into much less mobile ions. The integral of the current induced in the external circuit by the motion of these electrons and ions has a very distinctive waveform which is readily interpreted in terms of the total ion production rate. By judicious selection of mixture composition, conditions can be identified for which either ionization or attachment dominates ion production. This method with refinements has recently been used in the study of attachment reactions in a number of halogen bearing molecules. A review[19] of this work by Nygaard, Brooks and Hunter describes a typical apparatus and analysis of experimental waveforms.

B. Apparatus

Measurement Cell

A partial schematic of the swarm experiment used in this investigation is shown in Fig. 4. A spherical glass cell was provided with a quartz window permitting introduction of a UV light pulse, and with a set of identical planar electrodes for collection of ions and electrons. A vertical closed end tube attached to the cell bottom served as the $HgBr_2$ reservoir; a temporary glass appendage used to load $HgBr_2$ into the reservoir by vacuum distillation was later sealed off. To minimize reaction with $HgBr_2$, the collection electrodes were gold plated and the cell was isolated from gas and vacuum manifolds by a magnetically actuated ground glass valve.

The buffer gas pressure was measured with a capacitance manometer separated from the cell by a valve that was normally closed to minimize exposure to $HgBr_2$. The concentration of mercuric bromide was determined from its vapor pressure[10] at the reservoir temperature which was maintained by an oil bath. The cell itself was electrically shielded by multiple layers of aluminum foil wrapped directly

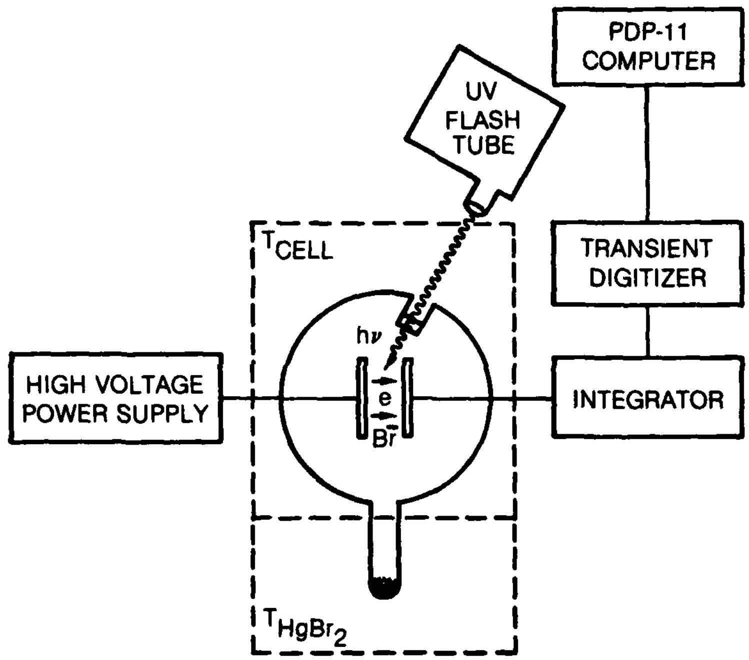

Fig. 4. Schematic illustration of the pulsed electron swarm experiment and related apparatus.

82-3-139-4

on the glass and superheated in a separate oven to control gas temperature. Thermocouples at three locations on the cell wall indicated a superheat temperature uniformity of better than 5°K at 420°K.

$HgBr_2$ Production

The presence of even very small amounts of molecular impurities can have a pronounced effect on measured transport properties. For this reason mercuric bromide was synthesized by the reaction of an excess of bromine (99.999) with mercury (99.99999) at 60°C and then vacuum distilled three times before distillation transfer to the gas reservoir. The glass transfer tube was then sealed and this was followed by a final vaporization in vacuum.

Current Integrators

The electrodes were 2.5 cm in diameter and were fixed at a separation of 1.5 cm. Connected to the emitting electrode was a well-regulated dc power supply. The collecting electrode was connected through either of two integrating circuits to a Tektronix transient digitizer PDP-11 computer combination. Single pulse or averaged waveforms could be recorded; most of the data were obtained by averaging 64 waveforms for signal/noise improvement. The integration of the electron component of this small signal was performed on the 80 pf net capacitance of a short length of RG58 coaxial cable and the input capacitance of the amplifier plug-in. Typical electron transit times were several microseconds during which time a signal of several millivolts was developed on this integrator.

The 80 μsec RC time constant of the fast integrator made it unsuitable for observation of the ion component of the swarm signal which had a characteristic time scale of about lmsec. However, the overall behavior of the swarm waveform was readily handled using an operational amplifier-based integrator with a feedback capacitor of 60 pf and a time constant of tens of milliseconds. Thus, electron transit times were determined from the fast integrator signal and the relative contributions of electron and ion components were obtained using the second integrator circuit. Typical integrated waveforms for electron and ion currents obtained with the transient digitizer (average of 64 waveforms) are shown in Fig. 5.

Photon Sources

The photon source used in these studies was an EG&G FX-265 bulb-type xenon flashtube. Use of a 0.05 pf low inductance capacitor in the manufacturer's recommended circuit resulted in photoflashes of approximately 600 nsec duration and of sufficient UV yield to provide the 10^6 photoelectrons required experimentally; larger quantities of photoelectrons caused space charge distortion of the applied electric field.

C. Analysis of Current Waveforms

The pulsed swarm experiment is idealized by considering the electrons to move as a sheet between the two electrodes under the influence of an applied electric field. At pressures where gas collisions dominate and when the electron concentration is sufficiently low to avoid space charge effects, the electron drift velocity and the electron energy distribution are characterized by the gas mixture and the prevailing electric field-to-gas density ratio, E/n. When attaching species are present in sufficient concentration in the gas mixture, and when the value of E/n is sufficient to ensure the presence of electrons at energies above the

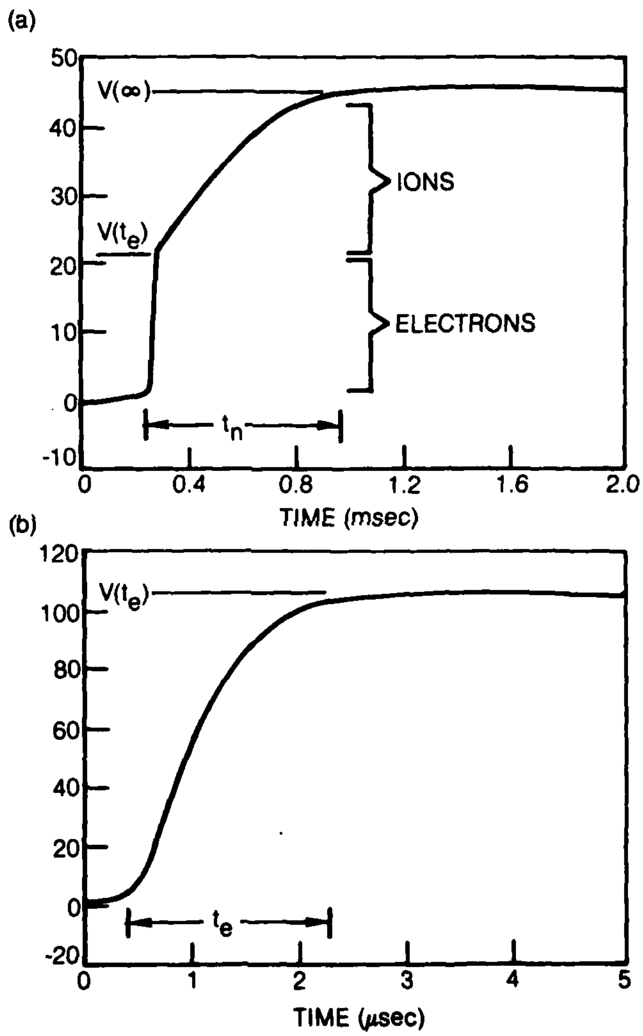

Fig. 5. Typical integrated waveforms for the ion (a) and electron (b) currents obtained with the transient digitizer as discussed in the text. The ion transit time, t_n, and electron transit time, t_e, are indicated.

82-3-139-5

threshold for attachment, conversion of electrons to negative ion will take place[19]. Under these conditions, an exponential attenuation of the number of electrons in the sheet will occur as it sweeps across the gap. Left behind will be a spatially distributed group of negative ions which also slowly drifts toward the collector. The current induced in the external circuit as a result of the motion of these charges consists of an initial several microsecond electron spike superimposed on a slowly declining, low current component due to the less mobile negative ions. Integration of this induced current waveform has two practical benefits. First, it converts the fast, low-level current pulse into an experimentally observable voltage waveform and secondly, it makes the extraction of the attachment rate data especially straightforward.

A typical integrated waveform is displayed in Fig. 5a. The leading edge of a similar waveform is shown in Fig. 5b on an expanded time scale. Note that the initial rapid rise of the integrated current to a voltage level $V(t_e)$ ends at the electron transit time, t_e. This time corresponds to electrode separation, L, divided by the electron drift velocity, v_{de}, i.e.:

$$t_e = L/v_{de} \quad . \tag{2}$$

A further slow increase in voltage follows until the last negative ions reach the collector from their origin near the emitter. At this time, which corresponds to the electrode separation, L, divided by the negative ion drift velocity, v_{dn}, i.e.,

$$t_n = L/v_{dn} \quad , \tag{3}$$

the current integral has attained its saturated value, $V(\infty)$. Mathematical modeling of the electron and negative ion currents and evaluation of their integrals reveals that the attachment rate coefficient, k_a, the concentration of the attaching gas, N_a, and the electron transit time, t_e, are related to the observed voltages $V(t_e)$ and $V(\infty)$ by the expression[19]:

$$\frac{V(t_e)}{V(\infty)} = \frac{1-e^{-k_a N_a t_e}}{k_a N_a t_e} \tag{4}$$

Thus, measurement of the two voltages $V(t_e)$ and $V(\infty)$ and the electron transit time t_e, along with a knowledge of N_a permits determination of k_a, the attachment rate coefficient. A more complex expression[19] for this voltage ratio applies when volume ionization augments the number of electrons in the swarm. However, in the limit where ionization greatly exceeds attachment, the shape of the integrated current is similar to that associated with attachment and:

$$\frac{V(t_e)}{V(\infty)} = \frac{1-e^{-k_i N t_e}}{k_i N t_e} \tag{5}$$

where k_i is the mixture weighted ionization rate coefficient and N is the total concentration of neutral species. Experimentally, the onset of ionization is readily distinguishable owing to the rapid increase in the saturation level, $V(\infty)$, with increasing E/n.

D. Electron Drift Velocity Measurements

A key factor in the determination of the ion production coefficient as described above is accurate determination of the electron transit time, t_e, based on interpretation of the leading edge of the integrated current waveform (Fig. 5b). In order to evaluate the accuracy of the present swarm experiment, the electron transit time was measured for several gases and mixtures (not containing $HgBr_2$) for which the electron drift velocity is known or can be computed with high accuracy using known cross sections; gas pressure was varied in the 50-200 torr range. The corresponding electron drift velocity data so obtained are shown in Fig. 6. Also shown is the drift velocity computed using the expression[20],

$$v_{de} = -\left(\frac{2e}{m}\right)^{1/2} \frac{E/n}{3} \int_0^\infty \frac{u df/du}{Q_{em}} du \quad , \tag{6}$$

in which e and m are the electron charge and mass, E is the electric field intensity, n is the total number density of neutrals, f is the isotropic component of the electron energy distribution function, Q_{em} is the mixture weighted momentum transfer cross section, and u is the electron energy expressed in electron volts. The electron distribution function was determined by numerical solution[20] of the Boltzmann equation for a uniform medium using the known cross sections for Xe[21], Ne[22], and N_2[23]. Figure 6 shows that the agreement between the computed and measured drift velocity values is very good, a finding indicative of the degree to which the present experimental configuration simulates an infinite, uniform electron drift region. The particularly large increase in the drift velocity upon addition of 0.1% N_2 to Xe is a consequence both of the Ramsauer minimum in the Xe momentum transfer cross section[21] in the vicinity of 0.5 eV, and the resonance in the N_2 vibrational cross sections[23] near 2.0 eV. For E/n values of a few Tds in the Xe + 0.1% N_2 mixture, resonant vibrational excitation of N_2 results in a mean electron energy

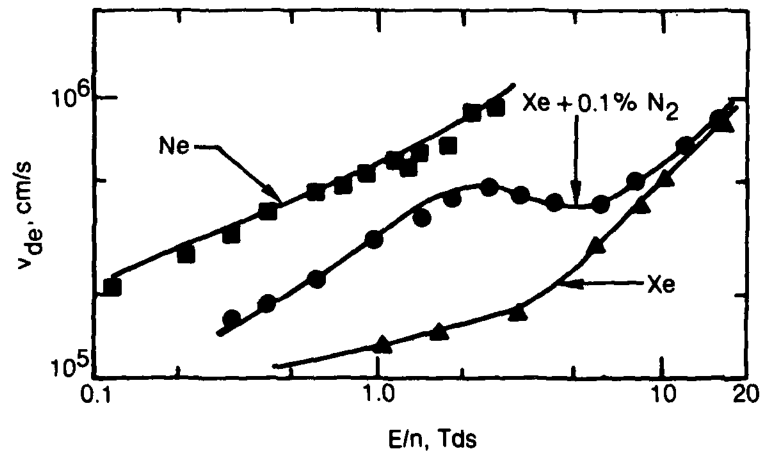

Fig. 6. Measured and computed electron drift velocity at 300°K. The drift velocity was measured at several pressures in the 50-200 Torr range and exhibited no pressure dependence.

82-3-139-6

of a few tenths of an eV, an energy for which the Xe momentum transfer cross section is at its minimum. Since the drift velocity is inversely proportional to the momentun transfer cross section (Eq. 6), this results in an unusually large increase in the drift velocity even though the N_2 fractional concentration is only 0.001.

Drift Velocity in Xe-$HgBr_2$ Mixtures

Detailed measurements of electron drift velocity in Xe-$HgBr_2$ mixtures were carried out for a Xe pressure and temperature of 140 Torr and 140°C, respectively; these values specify a Xe neutral number density of about 3×10^{18} cm^{-3}. Data were obtained for three $HgBr_2$ reservoir temperatures corresponding to $HgBr_2$ fractional concentrations of 0.067, 0.135 and 0.25%. Figure 7 presents the E/n variation of the measured drift velocity for a mixture containing 0.135% $HgBr_2$. The error bars indicated in the figure are primarily the result of the uncertainty associated with determination of the electron transit time from the integrated current waveforms (Fig. 5b). Although the qualitative variation of the measured drift velocity in Xe containing 0.135% $HgBr_2$ is markedly different from that observed with about the same amount of N_2 in Xe (Fig. 6), the magnitude of the measured change in the drift velocity for E/n values of a few Tds is of the same order as that observed with 0.1% N_2 in Xe. Further, the change in the drift velocity as the $HgBr_2$ concentration was increased (or decreased) was readily apparent. Since the Xe:$HgBr_2$ concentration ratio is approximately 10^3 for these conditions, and since the momentum transfer cross section for Xe is relatively large even at its minimum value ($\sim 10^{-17}$ cm^2), the drift velocity in Xe-$HgBr_2$ mixtures is not significantly affected by e-$HgBr_2$

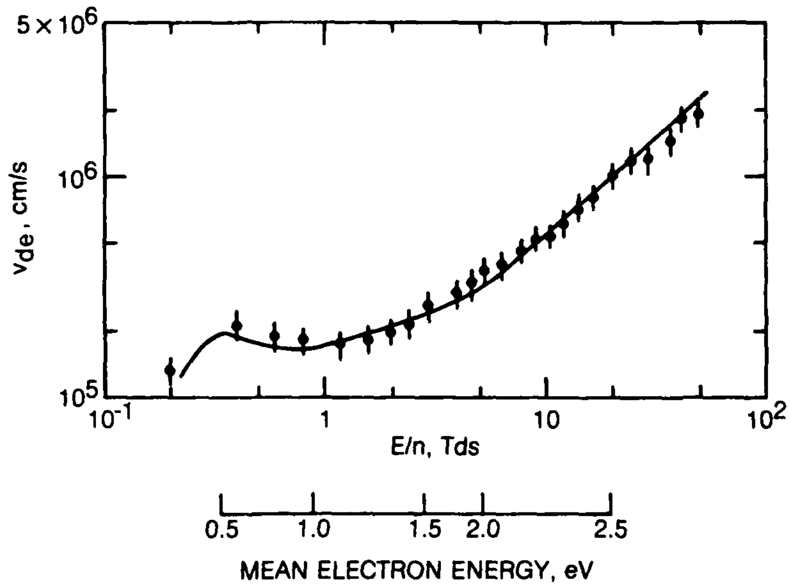

Fig. 7. Measured electron drift velocity in Xe at 140 Torr and 140°C containing 0.135% $HgBr_2$. Also shown is the drift velocity computed for this mixture using the cross sections shown in Fig. 12 as described in Sec. III-F of the text.

82-3-139-7

momentum transfer collisions. Rather, as is also the case for the Xe-0.1% N_2 mixture, the dependence of the drift velocity on $HgBr_2$ concentration reflects changes in the electron distribution function caused by low energy electron inelastic collisions with $HgBr_2$ (Eq. 6). The observed changes in the measured drift velocity can be interpreted on the basis of e-$HgBr_2$ vibrational excitation, a topic to be discussed in a subsequent section.

E. Ion Production Rate Measurements

Attachment in Xe-$HgBr_2$ Mixtures

The electron attachment coefficient for Xe-$HgBr_2$ mixtures was determined by employing Eq. 4 in conjunction with measured drift velocity data (i.e., the electron transit time) (Fig. 7) and corresponding measurements of the voltages $V(t_e)$ and $V(\infty)$, (Fig. 5a). Measured values of the attachment coefficient so determined are presented in Fig. 8, along with values computed using the attachment cross section of Fig. 3 and the expression[20],

$$k_a = \left(\frac{2e}{m}\right)^{1/2} \int_0^\infty u f Q_a(u)\,du \ . \qquad (7)$$

For the purposes of this and subsequent calculations of k_a the magnitude of the attachment cross section of Fig. 3 was reduced by 12%, an adjustment well within the estimated ± 30% accuracy of the measured cross section.

The strong dependence of k_a on E/n at the lower values of the latter reflects the interaction of the tail of the electron energy distribution and the threshold region of the attachment cross section (Fig. 3). For higher E/n values the bulk of the electrons have energies of a few eV, the region where Q_a peaks (Fig. 3),

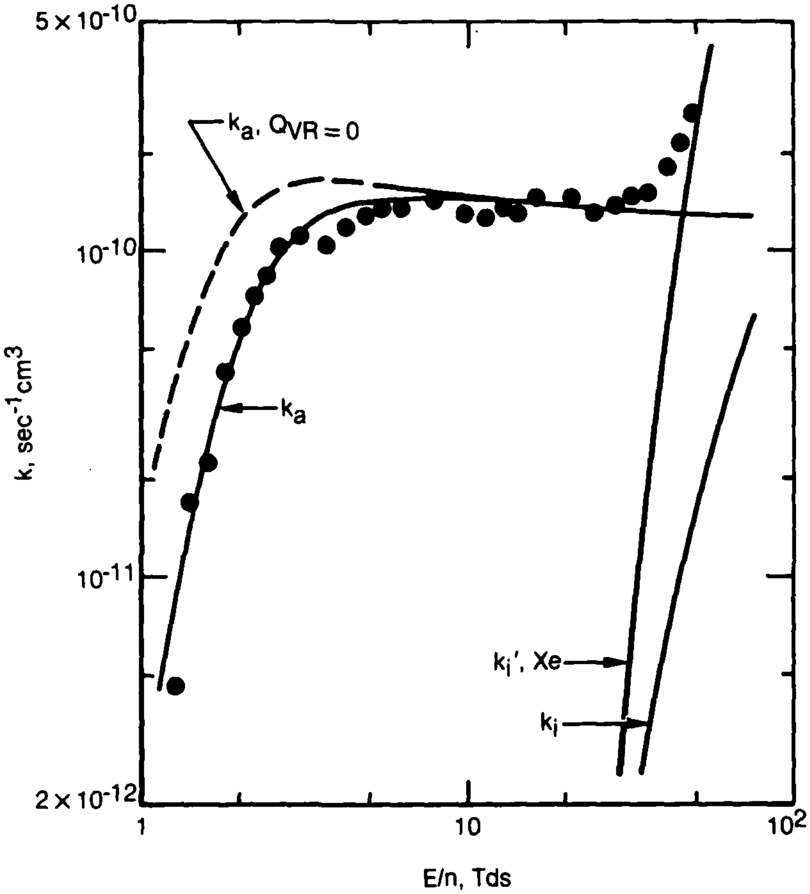

Fig. 8. Measured ion production coefficient for a Xe-0.135% $HgBr_2$ mixture at a total neutral number density of 3×10^{18} cm^{-3} and a temperature of 140°C. Also shown are computed rate coefficients for $HgBr_2$ attachment, k_a, and ionization, k_i, along with the Xe ionization coefficient, k_i', mixture weighted to account for the Xe/$HgBr_2$ concentration ratio. The attachment coefficient labeled $Q_{VR} = 0$ was computed neglecting resonant vibrational excitation of $HgBr_2$ as discussed in the text.

82-3-139-8

and the attachment coefficient reaches a plateau as indicated. Throughout the entire E/n region, the measured and computed attachment coefficients are found to be in very good agreement up to a value of about 30 Tds for this mixture. Recall, however, that the present measurement technique is sensitive to the total ion production rate, *not simply the production of negative ions*. Indeed, calculations show that the sharp increase in the measured ion production rate coefficient for an E/n value above approximately 35 Tds reflects the onset of Xe ionization rather than a change in the nature of the production of Br^- by way of the attachment reaction. Figure 8 shows that the computed value of the Xe^+ ion production coefficient, weighted to account for the Xe:$HgBr_2$ concentration ratio, is in excellent agreement with the observed increase in the measured total ion production coefficient for high E/n values. Comparison of the computed ionization rate coefficients for Xe and $HgBr_2$ shows that for this mixture the effect of Xe ionization is very much greater than that of $HgBr_2$.

Ionization in N_2-$HgBr_2$ Mixtures

Because of a rather fortuitous combination of circumstances, measurement of the ion production rate coefficient in N_2-$HgBr_2$ mixtures provides a means for determining the $HgBr_2$ ionization rate coefficient rather than the attachment rate coefficient. The reason for this can be understood by examination of Fig. 9 showing measured values of the total ion production coefficient and computed values of both the $HgBr_2$ attachment and ionization coefficient in an N_2-$HgBr_2$ mixture. Comparison of Figs. 8 and 9 reveals a marked qualitative and quantitative difference between the measured ion production coefficients and between the computed attachment coefficients in the N_2/$HgBr_2$ and Xe/$HgBr_2$ mixtures. Analysis of the calculated

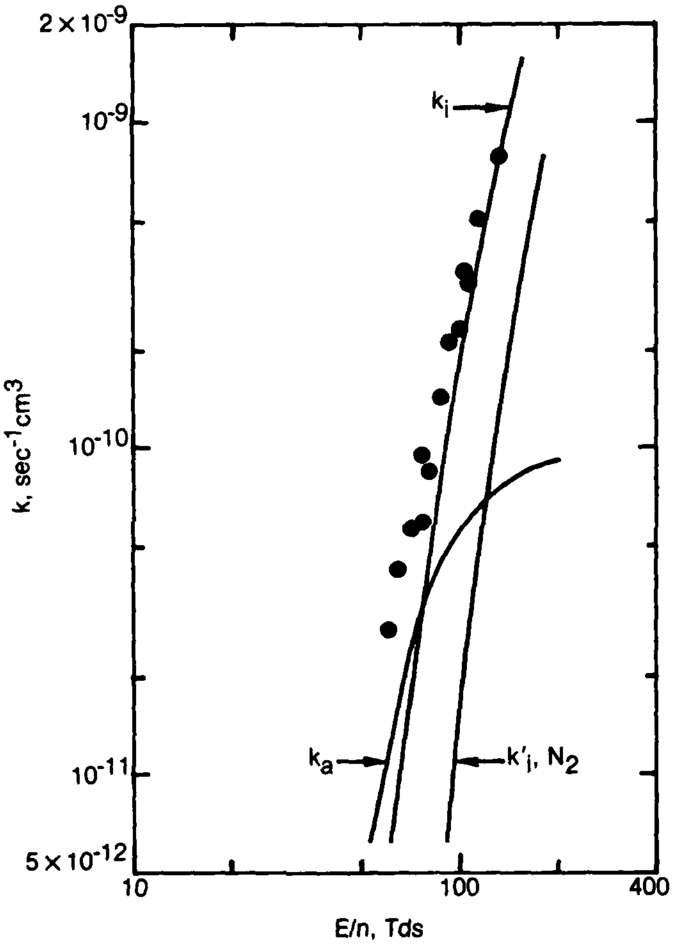

Fig. 9. Measured ion production coefficient for a N_2-2% $HgBr_2$ mixture at a total neutral number density of 1.9×10^{18} cm^{-3} and a temperature of 170°C. Also shown are computed rate coefficients for $HgBr_2$ attachment, k_a, and ionization, k_i, along with the N_2 ionization coefficient, k_i', mixture weighted to account for the $N_2/HgBr_2$ concentration ratio.

82-3-139-9

attachment coefficients shows that these differences are a reflection of important differences in the electron energy distribution functions for the two mixtures. For E/n values below about 50 Td in the $N_2/HgBr_2$ mixture, resonant vibrational excitation of N_2 results in a truncated electron energy distribution function[20,23] at an energy of about 2.0 eV, a value <u>less</u> than the 3 eV required for $HgBr_2$ dissociative attachment (Fig. 3). For this reason, at low E/n values the attachment rate coefficient is very much less in the $N_2/HgBr_2$ mixture than is the case for the $Xe/HgBr_2$ mixture. Indeed, the calculated rate coefficients of Fig. 9 indicate that by the time E/n is large enough in the $N_2/HgBr_2$ mixture to result in an attachment coefficient comparable to that of the $Xe/HgBr_2$ mixture ($\sim 10^{-10}$ sec^{-1} cm^3), direct ionization of $HgBr_2$ has already become the dominant $HgBr_2$ ion production process. As shown in Fig. 9, ionization of N_2 is not significant because of the high N_2 ionization potential and relatively small ionization cross section. Thus, for this mixture the swarm experiment provides a means for determination of the $HgBr_2$ ionization coefficient. Examination of Fig. 9 shows that the measured ion production coefficient in this $N_2/HgBr_2$ mixture is in very good agreement with the computed value of the $HgBr_2$ ionization rate coefficient, the latter obtained using Eq. 7 and the measured ionization cross section of Fig. 2.

<u>N_e-$HgBr_2$ Mixtures</u>

While the $HgBr_2$ attachment coefficient can be determined using Xe-$HgBr_2$ mixtures (Fig. 8) and the $HgBr_2$ ionization coefficient can be determined in N_2-$HgBr_2$ mixtures, <u>both</u> attachment and ionization of $HgBr_2$ are found to be important in Ne-$HgBr_2$ mixtures. Presented in Fig. 10 is the measured ion production rate coefficient in a Ne-$HgBr_2$ mixture for conditions similar to those for Figs. 8 and 9,

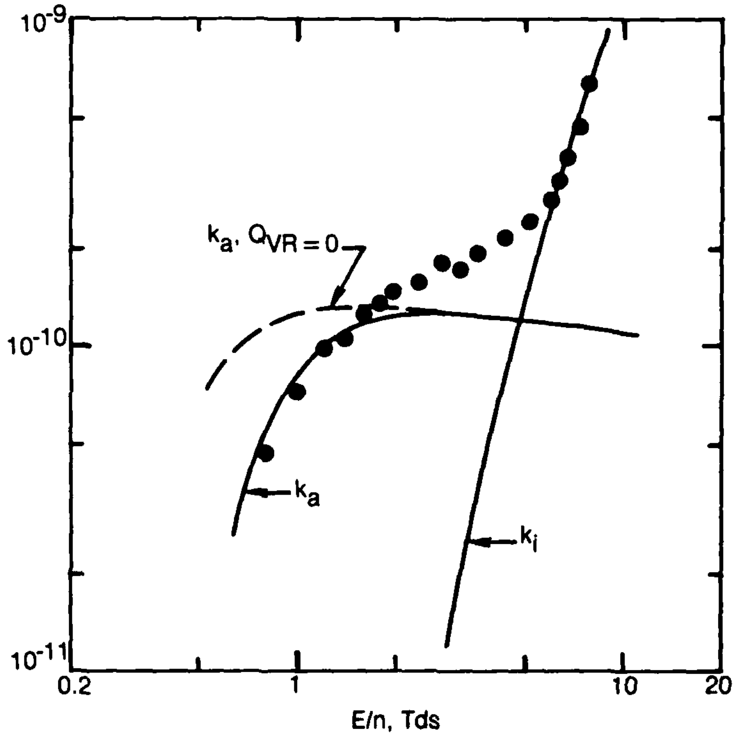

Fig. 10. Measured ion production coefficient for a Ne-0.2% $HgBr_2$ mixture at a total neutral number density of $3x10^{18}$ cm^{-3} and a temperature of 140°C. Also shown are the computed rate coefficients for $HgBr_2$ attachment, k_a, and ionization, k_i. The attachment coefficient labeled $Q_{VR} = 0$ was computed neglecting resonant vibrational excitation of $HgBr_2$ as discussed in the text.

82-3-139-10

along with computed values of the rate coefficients for attachment and ionization of $HgBr_2$. Ionization of Ne is insignificant for these conditions. Comparison of the experimental and analytical ion production coefficients shows that for this mixture attachment is dominant for E/n values below about 3 Tds and $HgBr_2$ ionization dominates for E/n above 5 Tds, with both processes contributing to ion production in the intermediate E/n regime.

Because Xe and N_2 have thresholds for electronic excitation which are below the 10.62 eV ionization potential of $HgBr_2$, and are present in much larger concentrations, the E/n value for which ionization becomes important in those mixtures (Figs. 8 and 9) is largely determined by the electronic cross sections of Xe and/or N_2. However, the threshold for electronic excitation in Ne is well above 10.62 eV, with the result that the E/n value for which $HgBr_2$ ionization becomes important in Ne-$HgBr_2$ mixtures is determined in large measure by the cross sections for $HgBr_2$ electronic excitation. For this reason the E/n variation of the measured ion production coefficient in Ne/$HgBr_2$ mixtures provides valuable information concerning the magnitude of the $HgBr_2$ cross sections for electronic excitation. Indeed, the $HgBr_2$ electronic cross sections used in the computation of k_a and k_i for the conditions of Fig. 10 were inferred on the basis of the present swarm measurements in conjunction with analysis of the properties of electron-beam controlled discharges in Ne-$HgBr_2$ mixtures[24]. These latter results will be reported elsewhere

F. Vibrational Excitation of $HgBr_2$

As discussed earlier in connection with Eq. 6 and Fig. 7, the electron drift velocity in atomic gases containing a small amount of a molecular additive is particularly sensitive to changes in the electron distribution function caused by inelastic electron collisions with the molecular species. Thus, when the qualitative and quantitative change in the drift velocity can be measured accurately over a wide range of conditions, the drift velocity itself can be used as a diagnostic to obtain information concerning the nature of the inleastic electron-molecule collision processes[21-23]. As part of the present study the observed changes in the drift velocity in Xe containing variable amounts of $HgBr_2$ were analyzed in order to investigate electron-$HgBr_2$ inelastic collision processes, particularly vibrational excitation.

Electron cross sections for electronic excitation of $HgBr_2$ have been recently inferred in connection with HgBr/$HgBr_2$ laser studies[24,25]. Although the inferred electronic cross sections are found to be large (> 10^{-17} cm^2), computation of the electron distribution function for the conditions of Fig. 7 using these $HgBr_2$ electronic cross sections alone shows that the resultant change in the drift velocity is quite a bit less than that measured in the present investigation, and that the qualitative variation of the drift velocity with E/n is substantially different from that observed. Additionally, the E/n dependence of the computed attachment coefficient in Xe and Ne-$HgBr_2$ mixtures differs substantially from measured values. The most probable explanation for such discrepancies is the effect of vibrational excitation of $HgBr_2$ on the electron energy distribution.

<u>Resonant e-$HgBr_2$ Vibrational Excitation</u>

Consideration of the large body of evidence on electron vibrational excitation of molecules indicates that, in general, vibrational excitation is likely to proceed by way of resonant electron capture by the molecule[23,26,27]. The intermediate resonant molecular negative ion state so formed subsequently decays through a number of exit channels resulting principally in vibrational excitation and dissociative attachment in those situations for which a stable negative ion can be formed. For this reason our observation of a resonant character in the $HgBr_2$ cross section for dissociative attachment provides a very valuable clue to the occurrence of resonant vibrational excitation of $HgBr_2$.

Figure 11 shows that the observation of a resonance in the attachment cross section in the 3-5 eV range is consistent with $HgBr_2^{*-}$ states likely to be formed[28,29] from HgBr and Br^-. This figure illustrates the two $HgBr_2^{*-}$ states that correlate with $HgBr(B^2\Sigma^+)$ and $HgBr(A^2\Pi)$ respectively. Indeed it has been suggested[30] that the neutral fragment of $HgBr_2$ dissociative attachment is $HgBr(B^2\Sigma^+)$. However, interpretation of the $HgBr(B \rightarrow X)$ fluorescence characteristics in electron-beam controlled discharges[24] is inconsistent with that interpretation. Rather, resonant excitation of the lower energy $HgBr_2^{*-}$ state indicated in Fig. 11 is more likely, i.e.

$$e + HgBr_2 \rightarrow HgBr_2^{*-} \begin{array}{l} \rightarrow HgBr(A^2\Pi) + Br^- \\ \rightarrow HgBr_2(v) + e \end{array} \qquad (8)$$

On the basis of the preceding arguments trial cross sections for resonant $HgBr_2$ vibrational excitation were constructed for use in solution of the Boltzmann equation for the conditions of Figs. 7, 8 and 10 following the usual iterative procedure[22,23]. These trial cross sections were adjusted until satisfactory agreement between the measured and computed electron drift velocity and attachment coefficient was obtained. The computed curves shown in Figs. 7, 8 and 10 are the result of this procedure and the cross sections used in the calculation are

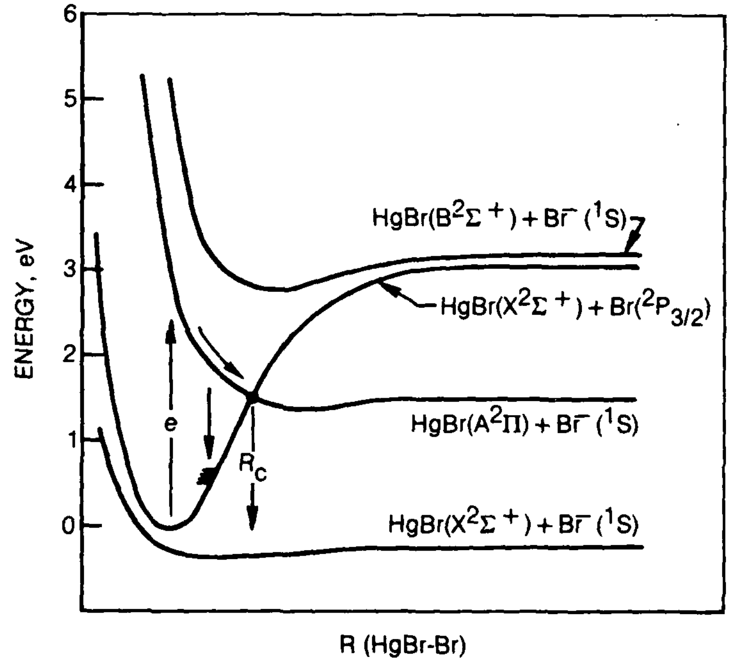

Fig. 11. Illustration showing representative $HgBr_2^{*-}$ potential energy curves. The two exit channels corresponding to $HgBr_2$ vibrational excitation and attachment following resonant excitation of the lowest energy $HgBr_2^{*-}$ state are illustrated. Dissociative attachment cannot occur unless the attached electron survives until the critical separation distance, R_c, is reached.

82-3-139-11

presented in Fig. 12. The effective electron energy loss used in conjunction with the resonant vibrational cross sectio, Q_{VR}, shown in Fig. 12 was 0.25 eV. Thus, the effective energy loss-cross section product of approximately 10^{-16} cm^2 eV is intended to reflect the combined effect of excitation of a great many $HgBr_2$ vibrational levels.

Figures 8 and 10 show that the strong increase in the computed attachment coefficient as E/n is increased is particularly sensitive to the nature of Q_{VR}. These figures show that for the lower E/n values the attachment coefficient computed using all $HgBr_2$ cross sections <u>except</u> Q_{VR} is a factor of two-to-three times higher than the measured values of the ion production coefficients. However, inclusion of the cross section Q_{VR} in the calculation depresses the tail of the electron energy distribution in the threshold region of the attachment cross section, significantly affecting the E/n variation of the attachment coefficient.

<u>Direct Vibrational Excitation</u>

Calculations show that the computed electron drift velocity in the Xe-$HgBr_2$ mixture of Fig. 7 is sensitive to the resonant portion of the vibrational cross section, Q_{VR}, in the 1.0-7.0 Td E/n range. Below about 1 Td Q_{VR} has very little effect on the drift velocity. Thus, in order to account for the observed distinctive drift velocity variation in Xe-$HgBr_2$ mixture for E/n below 1 Td (Fig. 7), a low energy electron $HgBr_2$ inelastic process, assumed to be direct (i.e., nonresonant) vibrational excitation, was taken into account.

Only the fundamental bending and asymmetric stretch modes[31] of $HgBr_2$, having excitation energies of 0.005 and 0.035 eV, have transition dipole moments. Thus, assuming that electric dipole scattering dominates nonresonant vibrational excitation,

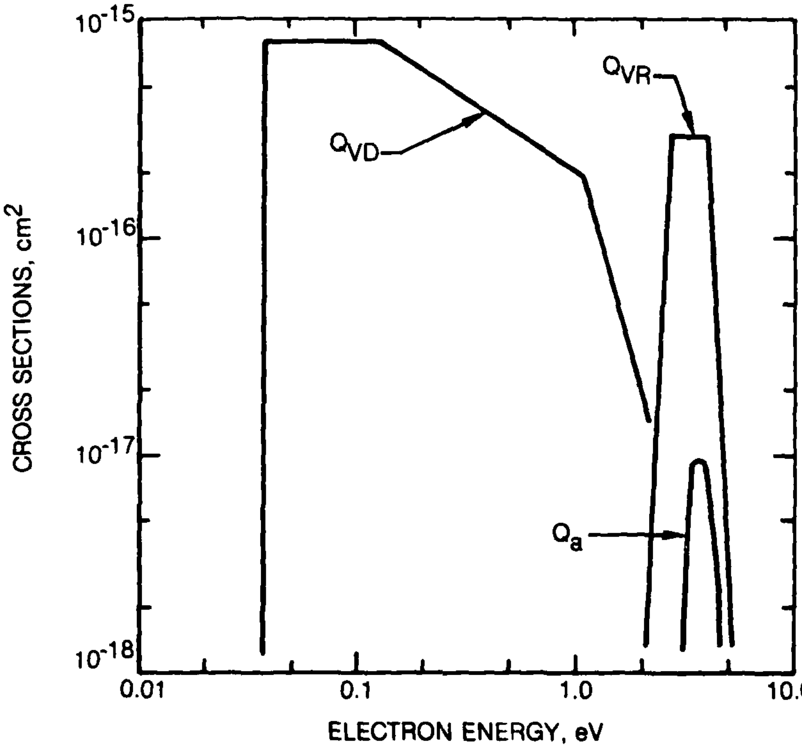

Fig. 12. Inferred cross sections for vibrational excitation of $HgBr_2$ by direct processes, Q_{VD}, having an energy loss of 0.035 eV, and by resonant excitation, Q_{VR}, with an effective energy loss taken to be 0.25 eV. The measured cross section for dissociative attachment (Fig. 3) is also shown for comparison.

82-3-139-12

only these modes are expected to have appreciable cross sections for electron energy well above threshold. However, calculations show that even the lowest E/n values of the present experiment correspond to mean electron energies very much higher than the 0.035 eV threshold of the asymmetric stretch mode. For this reason the present experimental data do not permit separation of direct vibrational excitation into its various components. Therefore, a single cross section, Q_{VD}, was used for analysis of the low E/n drift velocity data, having a threshold of 0.035 eV and the energy variation shown in Fig. 12. The magnitude of this cross section was adjusted until satisfactory agreement between the measured and computed drift velocity data for low E/n values in Xe-$HgBr_2$ mixtures was obtained (Fig. 7).

IV. SUMMARY

In this investigation an electron beam experiment has been used to measure the cross sections for $HgBr_2$ dissociative attachment and ionization to an accuracy estimated to be ±25%. The dominant ion products of these reactions have been determined from mass analysis to be Br^- and $HgBr_2^+$. Measurement of the total positive and negative ion production coefficients in several gas mixtures containing $HgBr_2$ using an electron swarm experiment has revealed dramatic differences in the nature of $HgBr_2$ related ion production processes (Figs. 8-10). Detailed analysis shows that the observed sensitivity of $HgBr_2$ ion production to the nature of the background gas is a manifestation of a sensitivity to the electron energy distribution. The sensitivity to the electron distribution function arises from the facts that the energy thresholds for $HgBr_2$ attachment and ionization are relatively high and low, respectively; and the electron cross sections for both processes are relatively large.

Very good agreement between measured and computed attachment coefficients is obtained over a wide range of E/n values and mixture conditions if vibrational excitation of $HgBr_2$ is taken into account. Indeed, the best agreement between measured and computed attachment coefficients and electron drift velocity data is obtained if it is assumed that vibrational excitation of $HgBr_2$ is dominated by a resonant excitation process in the 3-5 eV electron energy range for which dissociative attachment is also observed to occur. On the basis of this interpretation an effective cross section for resonant vibrational excitation of $HgBr_2$ has been determined by iterative solution of the Boltzmann equation for the conditions of the present experiments. The cross section so determined is assigned an energy loss of 0.25 eV so that the inferred peak cross section-energy loss product of approximately $1 \times 10^{-16} cm^2$ eV represents the combined effect of excitation of a great many $HgBr_2$ vibrational levels. The computed attachment coefficients and drift velocities are not unduly sensitive to specific details of either the magnitude of the vibrational cross section so inferred or the effective energy loss, so long as the energy loss-cross section product is about $10^{-16} cm^2$ eV and the effective cross section has an energy width of approximately 1-2 eV centered in the 3-4 eV range.

ACKNOWLEDGMENTS

It is a pleasure to acknowledge helpful discussions with our UTRC colleages R. T. Brown, H. H. Michels, and L. R. Boedeker, and with Professor D. W. Setser of Kansas State University and Professor A. Herzenberg of Yale University who provided valuable insight as to the likely nature of $HgBr_2$ vibrational excitation.

Additionally, the expert technical assistance of W. E. Conklin, J. A. Post and R. E. Cutting is greatly appreciated.

This work was supported in part by the Naval Ocean Systems Center and by the Office of Naval Research.

REFERENCES

1. R. Burnham and E. J. Schimitschek, Laser Focus _17_, 54 (1981); E. J. Schimitschek and J. E. Celto, Appl. Phys. Lett. _36_, 176 (1980): W. L. Nighan, Appl. Phys. Lett. _36_, 173 (1980).
2. W. J. Wiegand and L. R. Boedeker, Appl. Phys. Lett. _40_, 225 (1982).
3. J. T. Tate and P. T. Smith, Phys. Rev. _39_, 270 (1932).
4. D. Rapp and P. Englander-Golden, J. Chem. Phys. _43_, 1464 (1965).
5. D. D. Briglia and D. Rapp, J. Chem. Phys. _42_, 3201 (1965).
6. D. Rapp and D. D. Briglia, J. Chem. Phys. _43_, 1480 (1965).
7. P. J. Chantry, Phys. Rev. _172_, 125 (1968).
8. M. V. Kurepa and D. S. Belic, J. Phys. B _11_, 3719 (1978).
9. M. V. Kurepa, V. M. Pejcev and I. M. Cadez, J. Phys. D _9_, 481 (1976).
10. Vapor pressures for $HgBr_2$ were computed from the JANAF thermochemical tables (D. R. Stull and H. Prophet: Nat. Stand. Ref. Data Ser. _37_, (1971)) for the range of temperatures 300°K to 600°K. Pressure at 300°K is 1.2×10^{-4} torr and at higher temperatures is consistent with the tabular data listed by L. Brewer in: The Chemistry and Metallurgy of Miscellaneous Materials, Edited by L. L. Quill (McGraw-Hill, New York, 1950).
11. R. E. Fox, W. M. Hickam, D. J. Grove and T. Kjeldaas, Rev. Sci. Instrum. _26_, 1101 (1955).
12. P. J. Chantry, Rev. Sci. Instrum. _40_, 884 (1969).
13. H. M. Rosenstock, K. Draxl, B. W. Steiner and J. T. Herron, J. Phys. Chem. Ref. Data _6_, Suppl. 1, (1977).

REFERENCES (Cont'd)

14. R. E. Center and A. Mandl, J. Chem. Phys. 57, 4104 (1972).

15. F. W. Lampe, J. L. Franklin and F. H. Field, Jr., J. Amer. Chem. Soc. 79, 6129 (1957).

16. Landolt-Bornstein, Zahlenwerte and Functionen, 6 Auglange, Atom and Molecular-physik 3 Teil (Springer, Berlin, 1951), p. 514. The value of P_E reported therein was converted to polarizability α using the expression $\alpha = 0.3963 P_E$.

17. R. W. Kiser, J. G. Dillard and D. L. Dugger: Advan. Chem. Ser. 72, 153, (1968); The relative abundance of the product ions at 70 eV are: $HgBr_2^+$ (100.0), $HgBr^+$ (17.5), Br^+ (34.3), Hg^+ ($\sim$ 0) as listed in Ref. 17.

18. R. Grunberg, Z. Naturforsch. 24a, 1039 (1969).

19. K. J. Nygaard, H. L. Brooks and S. R. Hunter, IEEE J. Quantum Electron. QE-15, 1216 (1979).

20. W. L. Nighan, Phys. Rev. A 2, 1989 (1970).

21. L. S. Frost and A. V. Phelps, Phys. Rev. 136, A1538 (1964).

22. A. G. Robertson, J. Phys. B: Atom. Molec. Phys. 5, 648 (1972).

23. A. G. Engelhardt, A. V. Phelps and C. G. Risk, Phys. Rev. 135, A1566 (1964).

24. W. L. Nighan and R. T. Brown (to be published).

25. M. W. McGeoch, J. C. Hsia and D. E. Klimek (to be published).

26. G. J. Schulz, Rev. Mod. Phys. 45, 423 (1973).

27. D. Spence, J. L. Mauer and G. J. Schulz, J. Chem. Phys. 57, 5516 (1972).

REFERENCES (Cont'd)

28. H. H. Michels, private communication.

29. A. Herzenberg, private communication.

30. J. Degani, M. Rokni and S. Yatsiv, J. Chem. Phys. 75, 164 (1981).

31. W. Kelmperer and L. Lindeman, J. Chem. Phys. 25, 397 (1956).

April 14, 1982

Initial Distribution List

Director, Physics Program (Code 421) Office of Naval Research 800 North Quincy Street Arlington, Virginia 22217 Attn: Dr. M. B. White Ref.: Contract N00014-81-C-0253 Project: NR395-711/12-19-80	1 copy (with DD250)
Air Force Plant Representative Office Pratt & Whitney Aircraft, O.L.-AA East Hartford, CT 06108 Ref.: Contract N00014-81-C-0253 Project: NR395-711/12-19-80	1 copy
Director, Naval Research Laboratory Code 2627 Washington, D. C. 20375	6 copies
Defense Technical Information Center Bldg. 5, Cameron Station Alexandria, Virginia 22314	12 copies
Office of Naval Research Eastern/Central Regional Office Boston, Mass 02210	1 copy

Additional Copies

Dr. D. J. Schimitschek Code 811 Naval Ocean Systems Center 271 Catalina Blvd. San Diego, CA 92152	1 copy
Dr. R. Burnham Laser Physics Branch Naval Research Laboratory Washington, D. C. 20375	1 copy

Distribution List (Cont'd)

Dr. R. E. Behringer Office of Naval Research 1030 East Green Street Pasadena, CA 91101	1 copy
Dr. H. S. Pilloff Physics Program (Code 421) Office of Naval Research 800 North Quincy Street Arlington, VA 22217	1 Copy